applied optics

Implementation of a long range, distributed-volume, continuously variable turbulence generator

Gregory DiComo,[1,2,*] Michael Helle,[3] Joe Peñano,[3] Antonio Ting,[1,3] Andreas Schmitt-Sody,[4] and Jennifer Elle[4]

[1]Research Support Instruments, Lanham, Maryland 20706, USA
[2]University of Maryland, College Park, Maryland 20742, USA
[3]Plasma Physics Division, U.S. Naval Research Laboratory, Washington, DC 20375, USA
[4]U.S. Air Force Research Laboratory, Albuquerque, New Mexico 87101, USA
*Corresponding author: gregory.dicomo.ctr@nrl.navy.mil

Received 17 March 2016; revised 1 June 2016; accepted 2 June 2016; posted 2 June 2016 (Doc. ID 261287); published 27 June 2016

We have constructed a 180-m-long distributed, continuously variable atmospheric turbulence generator to study high-power laser beam propagation. This turbulence generator operates on the principle of free convection from a heated surface placed below the entire propagation path of the beam, similar to the situation in long-distance horizontal propagation for laser communications, power beaming, or directed energy applications. The turbulence produced by this generator has been characterized through constant-temperature anemometry, as well as by the scintillation of a low-power laser beam.

OCIS codes: (010.1330) Atmospheric turbulence; (010.1300) Atmospheric propagation; (010.7060) Turbulence; (030.7060) Turbulence.

http://dx.doi.org/10.1364/AO.55.005192

1. INTRODUCTION

A variety of laser applications have been considered which depend on long-distance atmospheric propagation of the beam to attain practical utility. Such applications include point-to-point laser communications [1], laser power beaming [2], and directed energy [3]. In each case, the effectiveness of the application is limited to some extent by beam distortions caused by atmospheric turbulence. Extensive effort has been devoted to modeling and experimentally investigating this phenomenon [4–9].

Experimental turbulence research can often be performed in the field, simply by allowing the laser to propagate across a long distance. The strength of optical turbulence is characterized by C_n^2, the coefficient of the structure function for the index of refraction. In the surface layer of the atmosphere, less than ~100 m above the ground, C_n^2 experiences daily variation over several orders of magnitude as the ground heats and cools with the rising and setting of the sun. A typical example of daily C_n^2 variation is given in Fig. 1. A large range of turbulence conditions can be sampled by observing the laser propagation throughout the day.

Many outdoor ranges suitable for long-distance laser propagation exist, including at Starfire Optical Range [12], the U.S. Naval Academy [13], across the Chesapeake Bay [14] and at the former space shuttle runway at Kennedy Space Center [15], among others. However, long-range outdoor experiments have the disadvantage of relying on uncontrollable natural variations, and the desired turbulence conditions may not occur during the experimental window. Many hours of experiment are required to secure a reasonable volume of data, which in any case will necessarily be under conditions which are not entirely known. In addition, laser safety considerations preclude the propagation of high-power beams at many outdoor ranges. Therefore, many techniques have been developed to generate or simulate turbulence in a more compact, more controllable manner in a laboratory setting [16]. These include a variety of fixed and variable phase screen methods, as well as turbulent fluid methods.

Fluid-based turbulence generators adopt perhaps the most direct approach to generating turbulence short of performing field experiments. A volume of air, water, or some other fluid is stirred through some combination of mechanical action (e.g., pumps, fans, jets) and thermal action (e.g., heat guns, hot plates, heater wires). Gradients in temperature result in turbulent fluctuations of the index of refraction. This method has several advantages: realistic Kolmogorov turbulence is naturally obtained; the strength of the turbulence is easily tuned by varying the strength of the heating; rare events such as intense

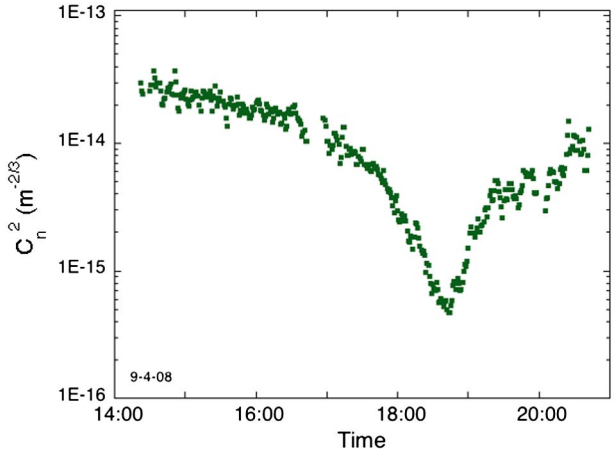

Fig. 1. Typical day of C_n^2 variation taken at Kirtland AFB, Albuquerque, NM. Data were taken through a differential image motion monitor (DIMM) [10], operating at a wavelength of 632.8 nm, on a clear day in early September 2008. Note the presence of a pronounced evening null event, and the accompanying rapid variation of the turbulence across several orders of magnitude. Over a distance of 2 km, the corresponding Rytov variance at that wavelength would range between 0.06 and 6.0 [11].

scintillations naturally occur with the appropriate frequency; the turbulence is distributed along the path rather than being tightly concentrated at one or a few longitudinal positions; appropriate construction materials are typically far cheaper than custom phase screens or deformable optics. The disadvantages are as follows: the inner and outer scales cannot be varied independently of C_n^2; the turbulence is truly random and cannot be reproduced except in a statistical sense; the generator occupies a large volume relative to phase screens; the heat used to generate the turbulence must be dissipated in some manner [16]. Turbulent fluid methods are well-suited for the study of high-power propagation because there are no physical optics, such as phase screens or spatial light modulators, which could be damaged by the high-power beam.

Previous fluid-based devices include that of Davis *et al.*, who developed a hot-water turbulence generator for creating turbulence on laboratory scales [17]. This uses a heating wire at the bottom of a water-filled acrylic tube to generate convection through a temperature differential. However, the turbulence evolves much more slowly than in air, and the inner scale is substantially larger than in air, owing to water's higher viscosity. Other groups have developed flow-driven [13,18,19] and convection-driven [20,21] hot-air turbulence generators, which generally produce distributed turbulence over a short distance, on the order of a few meters.

2. THEORETICAL BACKGROUND

In the lowest layers of the atmosphere near the surface, atmospheric turbulence is driven primarily by natural convection of hot air rising from the sun-warmed ground. A natural approach to generating artificial turbulence is therefore to heat some object placed below the propagation range and allow convection to drive turbulence. A long cylindrical heating element, such as a heating wire, allows the generation of turbulence along the beam's entire propagation path without consuming an unreasonable amount of power.

The behavior of flow due to natural convection is characterized by the nondimensional local Nusselt number, Nu, the ratio of convective to conductive heat transfer rates (q_{conv} and q_{cond}, respectively). For large values of Nu, convection dominates over conduction; for small values the reverse is true. Consider a layer of air of thickness x above a heated surface; the Nusselt number at the top of that layer is given by

$$\text{Nu}_x = \frac{q_{\text{conv}}}{q_{\text{cond}}} = \frac{h\Delta T}{\kappa \frac{\Delta T}{x}} = \frac{hx}{\kappa}, \tag{1}$$

where h is the geometry-dependent convective heat transfer coefficient in $\text{W/m}^2 \cdot \text{K}$, ΔT is the temperature difference between the heated surface and the ambient fluid, and κ is the thermal conductivity of the fluid in $\text{W/m} \cdot \text{K}$. The local Nusselt number increases with height above the source, as the air layer becomes thicker and conduction becomes less important compared to convection. Below a critical Nusselt number, between 100 and 1000, the flow remains laminar. Beyond this point, heat transfer is dominated by fluid motion, and the flow is considered to be turbulent.

Some difficulty lies in determining the convective heat transfer coefficient h, which is influenced by the geometry of the problem and the ability of air to flow around the heated surface. Experimentally determined correlating equations, relating the Nusselt number for the flow around a horizontal cylinder to other fluid mechanical parameters, have been developed by Churchill and Chu [22]. From their analysis, the convective heat transfer coefficient is given by

$$h_{\text{cyl}} = \frac{\kappa}{D}\left(0.6 + \frac{0.387\,\text{Ra}_D^{1/6}}{(1 + (0.559/\,\text{Pr})^{9/16})^{8/27}}\right)^2, \tag{2}$$

where Pr is the Prandtl number for air (0.713 at 20°C), Ra_D is the Rayleigh number for scale size D, and D is the diameter of the cylinder. The numerical factors have been determined experimentally through curve fitting over a wide range of Rayleigh numbers, $10^{-5} < \text{Ra}_D < 10^{12}$.

The nondimensional Rayleigh number, Ra, characterizes whether the flow around a heated object will be predominantly convective or conductive. The Rayleigh number for scale size x is given by

$$\text{Ra}_x = \frac{\rho g \beta \Delta T x^3}{\alpha \mu}, \tag{3}$$

where ρ is the density, g is the acceleration due to gravity, β is the coefficient of thermal expansion, α is the thermal diffusivity, and μ is the fluid's dynamic viscosity.

A laser beam propagating through a turbulent atmosphere will experience turbulence-driven phase distortions, resulting in beam wander, spreading, and scintillation. For fully developed turbulence with infinite Nusselt number, no deterministic behavior resulting from large-scale laminar flows remains. The foundational statistical treatment of such turbulence is generally held to be that of Kolmogorov [4]. Assuming a Kolmogorov turbulence spectrum, propagation in the weak fluctuation regime can be described using the Rytov method,

keeping only phase perturbations to second order. Under these conditions, the scintillation index (variance of intensity fluctuations) for a plane wave is given by the Rytov variance [7]

$$\sigma_R^2 = 1.23 C_n^2 k^{7/6} L^{11/6}, \tag{4}$$

where k is the angular wavenumber of the laser radiation, $k = \frac{2\pi}{\lambda}$, and L is the propagation distance.

3. OUTLINE OF METHODOLOGY

A. Turbulence Generation

At an indoor laser propagation range at the U.S. Air Force Research Laboratory, we have constructed and characterized a distributed turbulence generator, covering a propagation range of 180 m. To our knowledge, this comprises the world's longest continuously variable optical turbulence generator. The generator, pictured in Fig. 2, consists of a cluster of heating wires strung on steel cables running below the beam propagation path. Each wire is 73 m long. Tension on the steel cables and a series of quadrupeds positioned periodically along the path support the wires at a fixed distance below the beam. As the wires are heated, buoyant hot air from the wire convects upward to mix with the ambient air of the lab. Laboratory HVAC systems remove the excess heat and prevent the average temperature of the lab from increasing. Since the turbulence is driven by natural convective mixing, this method is more akin to a hot water chamber or a series of hot plates than it is to typical flow-driven hot-air turbulence generators. The strength of turbulence can be varied by adjusting the amount of power applied to the heater wires. The power consumed by the wires gives the rate of energy dissipation ϵ; this will enable comparison between the turbulence spectrum produced by the generator and theoretical predictions.

For the first set of experiments, two wires were strung 20 cm below the beam propagation path; this separation can be adjusted from an arbitrarily small distance up to as much as 1 m. The 20 cm separation was chosen to provide a scintillation index of 1 for a helium-neon laser (He–Ne, $\lambda = 632.8$ nm) at the highest heater setting, 19 W/m per wire. Additional electrical capacity exists to increase the number of wires if necessary in future experiments. Under these conditions, the buoyant air flows more or less up across the beam; this is like having a weak transverse wind, in which case the Taylor frozen flow hypothesis is expected to apply [7].

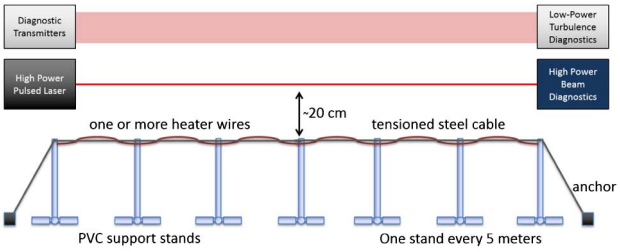

Fig. 2. Symbolic diagram of the turbulence generator. Heater wires strung on an extended framework running below the beam propagation path impart thermal and kinetic energy into the air, which naturally produces realistic Kolmogorov turbulence. Turbulence diagnostics copropagate with the laser beam, characterizing the turbulence as the experiment takes place.

The heater wires were measured to reach a temperature of 65 °C above ambient. The corresponding Nusselt number 20 cm above the wires is approximately 100. This is marginally within the range of Nusselt numbers considered to be characteristic of turbulent flow; therefore, the turbulence thus generated may not exhibit fully Kolmogorov statistics.

B. Turbulence Characterization

Three independent instruments were used to characterize the optical turbulence produced by the generator: a laser inner scale and scintillation diagnostic (LISSD), a commercial scintillometer, and a commercial optical anemometer. In addition, a constant temperature anemometer was used to characterize the spectrum of velocity fluctuations.

The LISSD was used to measure the structure parameter C_n^2 and the inner scale of turbulence l_0. This diagnostic was first developed and implemented by Consortini *et al.* in 2003 [23]. It uses a low-power He–Ne laser which propagates through the turbulence. The laser must have a Rayleigh range much shorter than the propagation distance, or a pinhole must be placed in front of the laser, to ensure that the wavefront at the detector is a spherical wave. The detector is a CCD positioned a fixed distance behind a pinhole. Scintillation and beam wander cause the spot formed on the CCD to fluctuate in both intensity and position. The intensity fluctuations are used to determine the scintillation index σ_I^2, which for a spherical wavefront in weak turbulence is equal to 0.4 times the Rytov variance. The position wander, coupled with the distance between the detector and the pinhole, gives the angle-of-arrival fluctuation $\langle \alpha^2 \rangle$. These two measurements give the path-averaged C_n^2 and l_0 according to

$$C_n^2 = \frac{2\sigma_I^2}{k^{7/6} L^{11/6}}, \tag{5}$$

and

$$l_0 = 1.08 L \left(\frac{\langle \alpha^2 \rangle}{\sigma_I^2} \right)^{1/2}. \tag{6}$$

For this experiment, the CCD camera used was an eight-bit color camera; this limited the size of the intensity fluctuations to a factor of 255.

A commercial scintillometer (Kipp & Zonen's LAS MkII) was used to benchmark the LISSD in a typical outdoor environment at the Naval Research Laboratory. Under these conditions, the C_n^2 values reported by the LISSD matched those reported by the commercial instrument. The scintillometer's operating wavelength of 850 nm is taken into account by its internal software when calculating C_n^2, so the wavelength difference between the LISSD and the scintillometer does not affect the measurement.

The scintillometer was also used during the indoor experiment. However, in the indoor experiment the turbulence was sometimes below the minimum detection threshold of the scintillometer; therefore, in this regime the results of the LISSD are considered to take precedence.

A commercial optical anemometer (OSI's long-baseline optical anemometer, or LOA) was available at the AFRL site: this instrument measures C_n^2 in addition to transverse wind speed. However, the LOA reported only very small values of C_n^2

during operation of the turbulence generator, on the order of 10^{-17} $m^{-2/3}$. This may be because the LOA's two optical paths were spaced out horizontally, whereas the air flow produced by the turbulence generator is vertical. A subsequent experiment with the LOA installed sideways produced results which demonstrated some response to the action of the turbulence generator. However, these results still did not reproduce the measurements of either the scintillometer or the LISSD.

In a separate experiment, a TSI constant-temperature anemometer (CTA) was used to characterize the velocity turbulence produced by the generator. The CTA was benchmarked by measuring the turbulent velocity fluctuations 1 m above a concrete parking lot. The structure function was generated by using the Taylor frozen-flow hypothesis to convert time-resolved data into space-resolved data. The one-dimensional power spectrum of the structure function demonstrated a slope of approximately $-5/3$, as expected for Kolmogorov turbulence, with a peak at high wavenumber corresponding to high frequency instrumental noise.

The coefficient of the velocity power spectrum, C_v^2, can be related to C_n^2, the gradient of the index of refraction, and the vertical gradient of the wind velocity [24]. Insufficient data were taken to perform this conversion. However, these results, summarized in Fig. 3, provide evidence that the turbulence generator is creating Kolmogorov turbulence similar to that encountered in a natural environment.

4. MODELING AND SIMULATION

To benchmark propagation models, we simulated the propagation of a low-power He–Ne laser beam through the turbulence generated at the AFRL range. Simulations were performed using the High Energy Laser Code for Atmospheric Propagation (*HELCAP*), a 4D (3D space + time) computer simulation code developed at NRL [25,26]. With the turbulence generator turned off, the initial divergence of the He–Ne laser beam was determined by measuring the laser spot size in the transmitter and receiver planes. The ambient turbulence was not sufficient to affect the beam divergence angle.

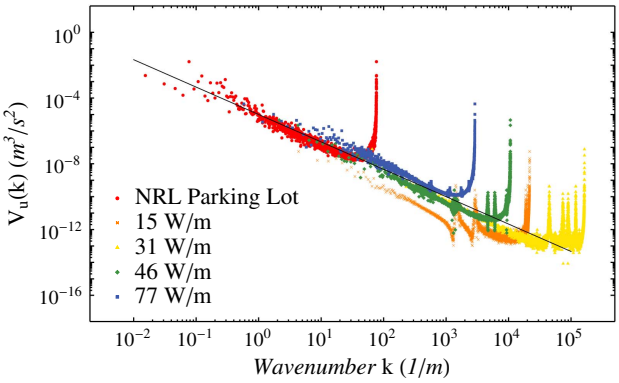

Fig. 3. One-dimensional velocity turbulence power spectra $V_u(k)$ for a naturally turbulent atmosphere (NRL parking lot, red), and four power density settings on the turbulence generator (orange through blue). A $-5/3$-slope line is displayed in black. High-wavenumber peaks on each data set represent high-frequency instrumental noise related to the oscilloscope sampling frequency.

With the initial divergence angle and spot size of the He–Ne beam established, C_n^2 and the inner scale were varied in the simulations according to the measured values. The simulated beam was propagated 180 m through the turbulence (assumed to be homogenous). *HELCAP* does not natively include buoyant convection; to mimic the effect of heat convection from the wires, a vertical wind was used in the simulation with speed equal to the buoyancy speed associated with the temperature of the wires.

Simulated beam images were compared with observed beam images in the receiver plane for various turbulence conditions (Fig. 4). Over the majority of the experiments, which produced a wide range of Rytov variances (both weak and strong turbulence regimes), it was observed that turbulence did not significantly increase the spot size of the beam in the receiver plane. Weak turbulence was observed to produce large-scale structures that convect across the beam, while strong turbulence produced smaller-scale filamentary structures. The same behavior was observed in the simulations, which were in good qualitative agreement with the experiments over the entire range of turbulence measured. This behavior is to be expected in the parameter regime for "case 3" of Fante's seminal paper [5], in which there is very little beam spreading, but high incoherence can occur. An example comparison of beam intensity in the receiver plane between experiments and simulations is shown in Fig. 4 for weak turbulence [$C_n^2 = 6 * 10^{-14}$ $m^{-2/3}$, $\sigma_I^2 = 0.15$, frames (a) and (c)] and strong turbulence [$C_n^2 = 5 * 10^{-13}$ $m^{-2/3}$, $\sigma_I^2 = 1.2$, frames (b) and (d)] cases.

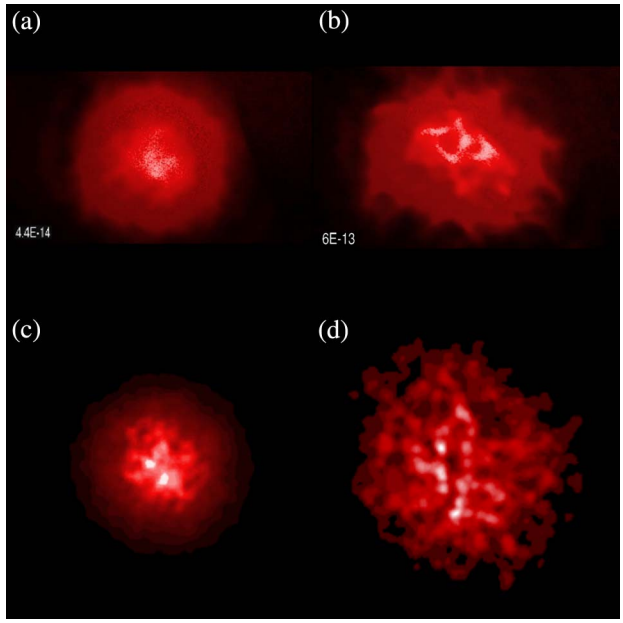

Fig. 4. Qualitative comparison between experimental and simulation results. (a) and (b) Still frames from video of laser beam scattered off target board in front of LISSD. (c) and (d) Still frames of animation produced in *HELCAP*. The spot size and fine beam structure observed in experiment are qualitatively reproduced in simulation. Low dynamic range of the camera prevents quantitative comparison of these images.

5. RESULTS

Measurements of the optical turbulence produced by the turbulence generator were performed at a variety of power levels, as well as with the facility HVAC system turned both on and off. The results are displayed in Figs. 5 and 6. At the maximum power level of 38 W/m, the intensity fluctuations caused dynamic range saturation in the LISSD detector; therefore, these data have been omitted.

With the HVAC system turned off, the turbulence in the propagation range is extremely weak, with C_n^2 as low as 10^{-16} $m^{-2/3}$ leading to a scintillation index as low as 10^{-4}. Activating the HVAC system increases this baseline level of turbulence by approximately an order of magnitude. At heater settings above 5 W/m, the turbulence produced by the turbulence generator dominates the natural turbulence of the facility, and the effect of the HVAC system becomes insignificant.

The scintillation index and angle-of-arrival fluctuations displayed in Fig. 5 are based directly on observation. The inner scale plotted in Fig. 5(b) has been calculated using Eq. (6), and holds under the conditions given by [23]; namely, that $L \ll l_0^2/\lambda$, and that the turbulence is Kolmogorov. Of these conditions, the first holds for all but the highest power settings. For a He–Ne laser and an inner scale of 1 cm, the limiting length is 158 m. This is on the order of our propagation distance; therefore, for the highest powers the actual inner scale may be somewhat smaller than depicted. The calculation of the Nusselt number (~100 at full power) gives us reason to believe that the second condition may not hold for lower power levels. However, anemometer measurements indicate that the turbulence generator produces a power spectrum similar to that of natural turbulence; see Fig. 3.

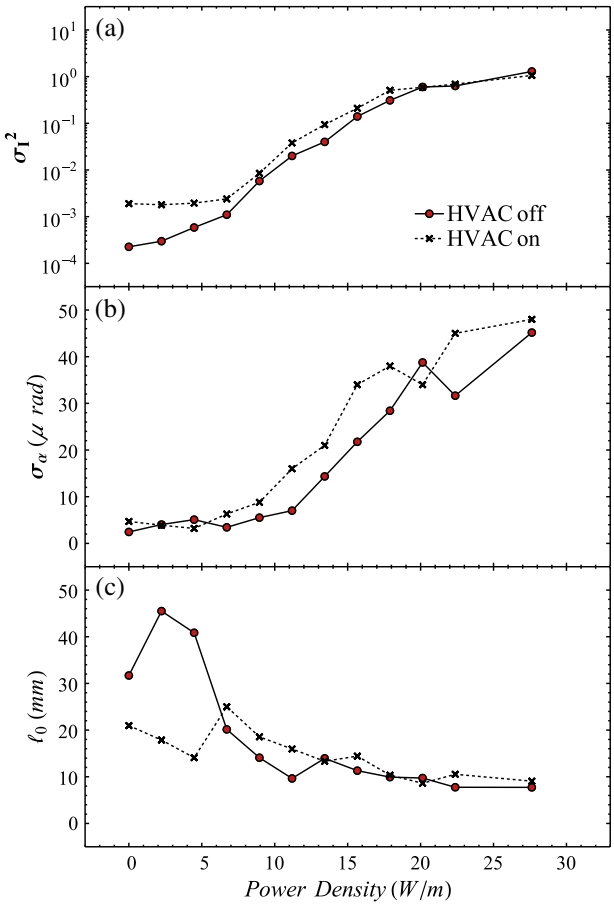

Fig. 5. Optical characterization of the turbulence generator through LISSD. (a) Scintillation index. (b) Standard deviation of the angle of arrival. (c) Inner scale, determined according to the method of Consortini, Eq. (6).

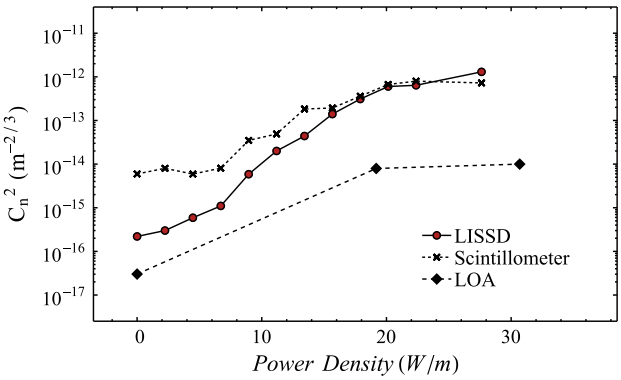

Fig. 6. Optical characterization of the turbulence generator through LISSD. The solid line represents the structure parameter C_n^2, as determined from LISSD scintillation data under the weak turbulence approximation, Eq. (5). The dotted line represents the C_n^2 output from the commercial scintillometer. The dashed line represents the results from the LOA diagnostic, performed during a separate experiment. The laboratory HVAC system remained off for this test.

The angle-of-arrival fluctuations and inner scales reported in Fig. 5 are averages of the x and y components determined by Consortini's method. A slight anisotropy exists: the y component is more often larger than the x component (23 out of 31 runs). On average, the y component of the angle-of-arrival fluctuations, and thus the inner scale in the y dimension, is 9.75% larger than the x component. This difference is too small to be visible in Fig. 5; therefore, only the average has been presented. The anisotropy may result from the average flow of air upward from the hot wires of the turbulence generator.

The C_n^2 values displayed in Fig. 6 are calculated under the assumption of weak Kolmogorov turbulence, and are therefore subject to the same conditions. The agreement between the LISSD-derived values and those obtained from the commercial scintillometer is observed to be excellent, except at the lowest turbulence intensities. The scintillometer performs a significant amount of space averaging by focusing a large collection aperture onto its internal detector; this renders the device resistant to large-amplitude scintillation saturation [27], but also averages out small fluctuations. This places a lower limit on the strength of the scintillations which the scintillometer can observe. The LISSD, which uses a small sampling aperture, does not have this limitation.

The C_n^2 reported by the LOA diagnostic is one to three orders of magnitude lower than that from the other two devices. These data were obtained with the LOA in the vertical orientation; oriented horizontally it was totally unresponsive to the action of the turbulence generator. In the vertical orientation, the increase in reported C_n^2 with increasing heater power

indicates that the device is operating. However, the LOA's failure to match the output of the LISSD or the scintillometer may indicate that transverse flow-measuring devices such as the LOA are inappropriate for measuring turbulence in such an environment.

6. CONCLUSION

A 180-m-long, continuously variable, distributed optical turbulence generator has been constructed and characterized. This device, to our knowledge the world's longest, has been shown to be capable of producing a scintillation index greater than 1 at a wavelength of 632.8 nm. The maximum scintillation index corresponds to an estimated maximum C_n^2 of $\sim 10^{-12}$ $m^{-2/3}$, and an inner scale l_0 of 8 mm. The strength of turbulence can be adjusted by increasing or decreasing the power delivered to the generator, as well as by varying the beam propagation height above the heating cables.

This turbulence generator can produce an environment similar to the convection-driven turbulence characteristic of the atmospheric surface layer, in a controlled laboratory environment. In addition, the generator could be used to characterize and study the turbulence produced by other line sources of heat, such as a high-energy laser beam propagating through an absorptive medium.

Based on calculation of the nondimensional Nusselt number, the turbulence generated by this method is considered likely to be Kolmogorov for the higher power settings. Comparison of the power spectrum produced by the generator to that observed in a natural environment reveals similar spectral characteristics even at low power levels. Further characterization will be performed as the turbulence generator is used in future experiments to investigate high power laser propagation.

Funding. Office of Naval Research (ONR); High Energy Laser-Joint Technology Office (HEL-JTO); U.S. Naval Research Laboratory Base Program.

Acknowledgment. The authors acknowledge Dr. Thomas Antonsen of the University of Maryland, College Park, for useful discussions, and the experimental assistance of Mr. Cameron Springer, a 2015 Directed Energy Scholar.

REFERENCES

1. R. Mahon, C. I. Moore, H. R. Burris, M. Ferraro, W. S. Rabinovich, M. Suite, and L. M. Thomas, "Probability density of irradiance fluctuations observed over terrestrial ranges," Appl. Opt. **50**, 6476–6483 (2011).
2. T. Blackwell, "Recent demonstrations of laser power beaming at DFRC and MSFC," in *BEAMED ENERGY PROPULSION: Third International Symposium on Beamed Energy Propulsion* (AIP, 2005), Vol. **766**, pp. 73–85.
3. P. Sprangle, B. Hafizi, A. Ting, and R. Fischer, "High-power lasers for directed-energy applications," Appl. Opt. **54**, F201–F209 (2015).
4. A. N. Kolmogorov, "The local structure of turbulence in incompressible viscous fluid for very large Reynolds numbers," Dokl. Akad. Nauk SSSR **30**, 299–303 (1941).
5. R. L. Fante, "Electromagnetic beam propagation in turbulent media," IEEE Proc. **63**, 1669–1692 (1975).
6. R. Williams and C. Paulson, "Microscale temperature and velocity spectra in the atmospheric boundary layer," J. Fluid Mech. **83**, 547–567 (1977).
7. L. C. Andrews and R. L. Phillips, *Laser Beam Propagation Through Random Media* (SPIE, 2005), Vol. **1**.
8. C. I. Moore, H. R. Burris, M. F. Stell, L. Wasiczko, M. R. Suite, R. Mahon, W. S. Rabinovich, G. C. Gilbreath, and W. J. Scharpf, "Atmospheric turbulence studies of a 16 km maritime path," in *Defense and Security* (International Society for Optics and Photonics, 2005), pp. 78–88.
9. J. Peñano, B. Hafizi, A. Ting, and M. Helle, "Theoretical and numerical investigation of filament onset distance in atmospheric turbulence," J. Opt. Soc. Am. B **31**, 963–971 (2014).
10. M. Sarazin and F. Roddier, "The ESO differential image motion monitor," Astron. Astrophys. **227**, 294–300 (1990).
11. R. Fischer, A. Ting, G. DiComo, J. Caron, C. Pogue, P. Sprangle, J. Peñano, and B. Hafizi, "Long-range propagation of high-power, single-mode fiber lasers," in *Directed Energy Professional Society Annual Symposium* (2009).
12. R. Q. Fugate, B. L. Ellerbroek, C. H. Higgins, M. P. Jelonek, W. J. Lange, A. C. Slavin, W. J. Wild, D. M. Winker, J. M. Wynia, J. M. Spinhirne, B. R. Boeke, R. E. Ruane, J. F. Moroney, M. D. Oliker, D. W. Swindle, and R. A. Cleis, "Two generations of laser-guide-star adaptive-optics experiments at the Starfire Optical Range," J. Opt. Soc. Am. A **11**, 310–324 (1994).
13. C. Nelson, S. Avramov-Zamurovic, R. Malek-Madani, O. Korotkova, R. Sova, and F. Davidson, "Measurements and comparison of the probability density and covariance functions of laser beam intensity fluctuations in a hot-air turbulence emulator with the maritime atmospheric environment," Proc. SPIE **8517**, 851707 (2012).
14. C. I. Moore, H. R. Burris, Jr., W. S. Rabinovich, L. Wasiczko, M. R. Suite, L. A. Swingen, R. Mahon, M. F. Stell, G. C. Gilbreath, and W. J. Scharpf, "Overview of NRL's maritime laser communication test facility," in *Optics and Photonics* (International Society for Optics and Photonics, 2005), p. 589206.
15. R. L. Phillips and L. C. Andrews, "Measured statistics of laser-light scattering in atmospheric turbulence," J. Opt. Soc. Am. **71**, 1440–1445 (1981).
16. L. Jolissaint, "Optical turbulence generators for testing astronomical adaptive optics systems: a review and designer guide," Publ. Astron. Soc. Pac. **118**, 1205–1224 (2006).
17. C. C. Davis, Y. Zhang, M. L. Plett, P. Polak-Dingels, P. R. Barbier, and D. W. Rush, "Characterization of a liquid-filled turbulence simulator," Proc. SPIE **3432**, 38–49 (1998).
18. A. K. Majumdar, J. A. DiUbaldo, and A. Brown-VanHoozer, "Laboratory simulation of atmospheric turbulence for laser propagation: design and characterization," Proc. SPIE **3432**, 50–56 (1998).
19. O. Keskin, L. Jolissaint, and C. Bradley, "Hot-air optical turbulence generator for the testing of adaptive optics systems: principles and characterization," Appl. Opt. **45**, 4888–4897 (2006).
20. R. Salamé, N. Lascoux, E. Salmon, R. Ackermann, J. Kasparian, and J.-P. Wolf, "Propagation of laser filaments through an extended turbulent region," Appl. Phys. Lett. **91**, 171106 (2007).
21. W. Nelson, J. P. Palastro, C. Wu, and C. C. Davis, "Enhanced backscatter of optical beams reflected in turbulent air," J. Opt. Soc. Am **32**, 1371–1378 (2015).
22. S. W. Churchill and H. H. Chu, "Correlating equations for laminar and turbulent free convection from a horizontal cylinder," Int. J. Heat Mass Transfer **18**, 1049–1053 (1975).
23. A. Consortini, Y. Y. Sun, C. Innocenti, and Z. P. Li, "Measuring inner scale of atmospheric turbulence by angle of arrival and scintillation," Opt. Commun. **216**, 19–23 (2003).
24. S. Fiorino, "Satellite and radar measurement of C_T^2, C_n^2, and C_v^2," in *Propagation Through and Characterization of Distributed Volume Turbulence*, (Optical Society of America, 2014), paper PM1E–1.
25. P. Sprangle, J. Peñano, and B. Hafizi, "Propagation of intense short laser pulses in the atmosphere," Phys. Rev. E **66**, 046418 (2002).
26. J. Peñano, P. Sprangle, B. Hafizi, A. Ting, D. Gordon, and C. Kapetanakos, "Propagation of ultra-short, intense laser pulses in air," Phys. Plasmas **11**, 2865–2874 (2004).
27. T.-i. Wang, G. R. Ochs, and S. F. Clifford, "A saturation-resistant optical scintillometer to measure c_n^2," J. Opt. Soc. Am. **68**, 334–338 (1978).